



Power Electronic Systems
Laboratory

© 2020 IEEE

IEEE Transactions on Power Electronics, Vol. 36, No. 4, pp. 4066-4080, April 2021

Analysis of the Influence of Measurement Circuit Asymmetries on Three-Phase CM/DM Conducted EMI Separation

P. Niklaus,
M. Antivachis,
D. Bortis,
J. W. Kolar

Personal use of this material is permitted. Permission from IEEE must be obtained for all other uses, in any current or future media, including reprinting/republishing this material for advertising or promotional purposes, creating new collective works, for resale or redistribution to servers or lists, or reuse of any copyrighted component of this work in other works.



Eidgenössische Technische Hochschule Zürich
Swiss Federal Institute of Technology Zurich

Analysis of the Influence of Measurement Circuit Asymmetries on Three-Phase CM/DM Conducted EMI Separation

Pascal S. Niklaus, *Student Member, IEEE*, Michael M. Antivachis, *Student Member, IEEE*,
 Dominik Bortis, *Member, IEEE*, and Johann W. Kolar, *Fellow, IEEE*

Abstract—Electromagnetic Interference (EMI) Conducted Emissions (CE) are of increasing concern in power electronics due to the high switching frequency and fast switching speeds of the latest generation of wide-bandgap semiconductors. The decomposition of the total conducted EMI noise into its Common-Mode (CM) and Differential-Mode (DM) part by means of a CM/DM noise separator is a useful tool that allows for a systematic EMI filter design. Carefully designed realizations achieve a Common-Mode Rejection Ratio (CMRR) and Differential-Mode Rejection Ratio (DMRR) of 50 dB at 30 MHz. However, a very high performance CM/DM noise separator is not sufficient. It is theoretically analyzed and experimentally proven that asymmetries in the EMI test setup result in an unwanted conversion between CM and DM EMI noise and therefore significantly influence the CM/DM EMI separation. In particular, three main influences are identified: the Line Impedance Stabilization Network (LISN), the connection cables between LISN and the Equipment Under Test (EUT) and the converter EMI filter. The unwanted noise conversion is pronounced for frequencies in the MHz range, where parasitic resonances occur. Experimental results show a CM-to-DM conversion of up to -30 dB at 30 MHz (a degradation by 20 dB or a factor of 10 compared to a high performance separator alone) considering a connection cable length mismatch of roughly 5 cm. Values as high as -21 dB result when standard commercial LISNs are used for the measurement. The impact of asymmetries in the EMI filter is most severe and clearly limits the EMI noise splitting at high frequencies. A high performance noise separator can, however, be used to investigate such filter asymmetries (component tolerances and/or layout) and therefore helps to improve the filter design process and facilitates the modeling of EMI noise sources.

Index Terms—common-mode (CM) and differential-mode (DM) noise separation, electromagnetic compatibility (EMC), electromagnetic interference (EMI), EMI measurements, line impedance stabilization network (LISN), EMI filter optimization, three-phase CM/DM noise separator.

I. INTRODUCTION

POWER electronic converter systems connected to the public mains must comply with international standards on Electromagnetic Compatibility (EMC) such as CISPR 11 [1] for industrial, scientific and medical equipment. EMC standards mandate the maximum allowed Electromagnetic Interference (EMI) noise spectral components in a certain frequency band. The regulations distinguish between Conducted

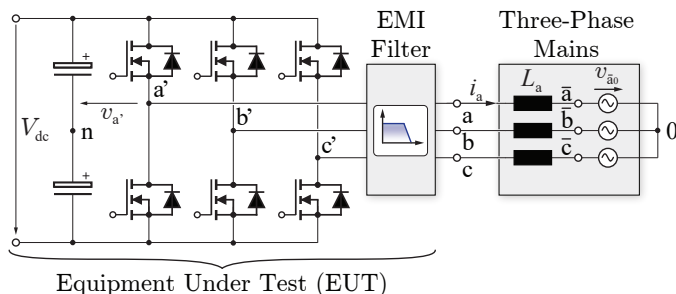


Fig. 1. Equipment Under Test (EUT): Photovoltaic three-phase inverter system with output filter, that supplies energy to the three-phase public mains (here shown with idealized sinusoidal voltage sources v_{i0} and corresponding inner mains inductances L_i , $i \in \{a, b, c\}$).

Emissions (CE) evaluated in the frequency band between 150 kHz and 30 MHz, and Radiated Emissions (RE) evaluated between 150 kHz and 1 GHz. RE can be relatively easily mitigated by placing the converter within a metallic enclosure, as it is usual practice in industrial applications. Of specific relevance for power electronic designs are typically the CE, which are measured using a Line Impedance Stabilization Network (LISN) according to CISPR 16-1-2 [2]. The LISN acts as interface between the Equipment Under Test (EUT), i.e., the converter system that has to fulfil the regulations (cf. **Fig. 1**), and the mains. In a standard CE EMI test setup the EUT is connected to the three-phase mains and an EMI test receiver with help of a three-phase LISN (dotted line in **Fig. 2**). The LISN provides a standardized inner mains impedance seen by the EUT [2] and allows to measure the EUT generated conducted EMI noise appearing at the LISN High-Frequency (HF) output ports (voltages $v_{LISN,i}$). Furthermore, the LISN decouples the EUT from any HF noise present in the supplying mains and decouples the HF output port from any Low-Frequency (LF) power flow related components that would destroy the sensitive EMI measurement equipment given their large magnitude. The standard setup, however, does not distinguish between Common-Mode (CM) and Differential-Mode (DM) EMI noise. The LISN voltages contain both, CM and DM voltage components. Therefore, if for example, the measured EMI noise exceeds the mandated regulation limits, the designer does not know if this is caused by the CM or DM noise component. Accordingly, it is difficult

This paper was **not** presented on any previous conference.

Corresponding Author: Pascal S. Niklaus

P. S. Niklaus, M. Antivachis, D. Bortis and J. W. Kolar are with the Power Electronic Systems Laboratory, Swiss Federal Institute of Technology, Zurich 8092, Switzerland (e-mail: niklaus@lem.ee.ethz.ch; antivachis@lem.ee.ethz.ch; bortis@lem.ee.ethz.ch; kolar@lem.ee.ethz.ch).

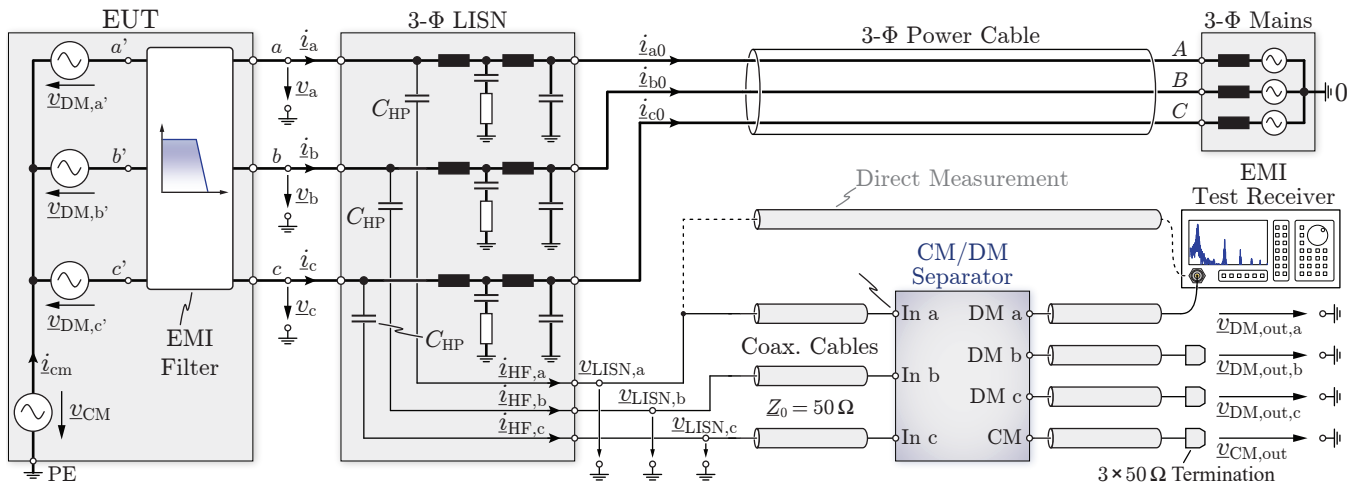


Fig. 2. Typical EMI pre-compliance measurement setup for a three-phase EUT using a three-phase CM/DM noise separator.

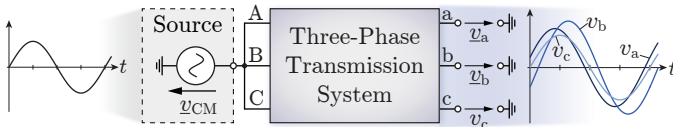


Fig. 3. Schematic representation of amplitude and phase mismatch in a three-phase transmission system with nominally identical transfer characteristics from each input A, B, C to the corresponding output a, b, c for a purely CM input voltage.

to assess if the DM or CM part of the EMI filter is underperforming and/or needs to be redesigned.

For this reason, a precompliance EMI test is often performed with the goal to also distinguish between the CM and DM EMI noise. An extension of the standard EMI test setup as shown in **Fig. 2** includes a CM/DM noise separator (highlighted in blue), which separates the three noise voltages $v_{LISN,i}$ into one CM and three DM components ($v_{CM,out}$ and $v_{DM,out,i}$). Coaxial cables with a characteristic impedance of $50\ \Omega$ are employed for the signal connections. Only one voltage at a time can be measured with typical EMI test receivers so any unused HF output terminal must be terminated with $50\ \Omega$. The detailed insight in the noise behavior enables selective adjustments of the CM and DM filter stages of the EMI filter to ensure compliance with the respective norms. Furthermore, CM and DM EMI noise equivalent circuits can be verified when comparing simulations and measurements. In order to perform an accurate separation a noise separator with very high separation capability, i.e., without cross-conversion of CM input noise to DM output noise (CM-to-DM conversion) and vice versa is required.

It has been shown in literature [3]–[6] that to achieve the demanded high separation capability for three-phase noise separators a highly symmetric layout and close matching between the three phases is of paramount importance. Asymmetries and insufficient matching manifest themselves in a deviation of the amplitude and/or phase from the desired nominal values. **Fig. 3** shows a three-phase transmission system (highlighted in blue) with nominally identical transfer functions from each input $A,$

B, C to the corresponding outputs a, b, c . A pure CM input voltage is assumed and the amplitude and phase mismatch resulting from the imperfectly matched transfer functions in the three-phase transmission system are highlighted. The three output voltages v_a, v_b and v_c are not entirely CM anymore but also contain a certain DM component. Therefore, a CM-to-DM conversion has taken place.

In noise separators the parasitic CM-to-DM conversion (and vice versa) is characterized with the Common-Mode Rejection Ratio (CMRR) and Differential-Mode Rejection Ratio (DMRR). It is clear, however, that not only the noise separator but all parts of the extended CE EMI test setup according to **Fig. 2** are potential sources of mismatch that could lead to parasitic CM-to-DM conversion (and vice versa). Only with a very high performance CM/DM noise separator, however, there is the confidence that any measured CM-to-DM conversion (and vice versa) is not caused by the noise separator itself but can be reliably attributed to the previously listed causes.

A. Overview of this Work

In this work, various sources of mismatch in the CE EMI test setup that impair the overall noise separation performance are identified and analyzed. Quantitative results that indicate the maximum achievable separation capability for a given mismatch are provided. Firstly, in **Section II** the EMI noise equivalent circuit of a standard Voltage Source Inverter (VSI) is presented, followed by a short review of existing three-phase noise separators with the achieved separation performance. **Section III** then theoretically discusses the CM-to-DM conversion resulting from certain amplitude and/or phase mismatches in a three-phase transmission system. The experimentally determined CM-to-DM conversion caused by asymmetries in the connecting cables and the LISN is quantified in **Sections IV** and **V**, respectively.

Finally, **Section VI** analyzes a three-phase CM and DM EMI filter stage and it is shown that already small mismatches between the three phases are causing a significant conversion from CM noise to DM noise. All theoretical considerations are

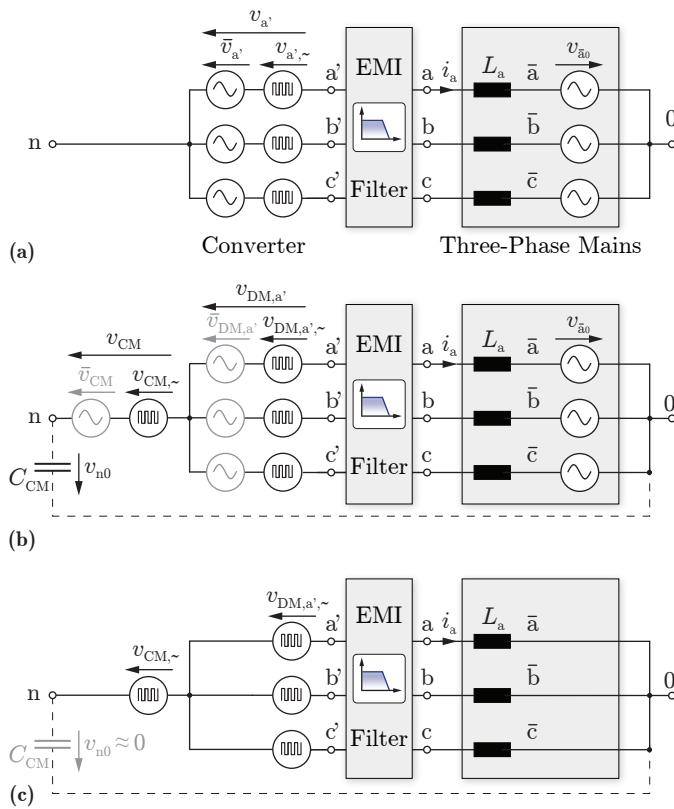


Fig. 4. Simplified representation of the three-phase inverter with EMI filter of **Fig. 1** using equivalent voltage source circuits. **(a)** Three switch-node voltages $v_{a'}$, $v_{b'}$ and $v_{c'}$ with a (desired) fundamental frequency component \bar{v}_i and a high frequency switching component $v_{i,\sim}$ and **(b)** further decomposition of both frequency components into CM and DM parts. **(c)** Only the EMI relevant high-frequency components are considered for the worst-case with $v_{n0} = 0$.

verified by means of experimental measurements. In summary, the sensitivity of the CE EMI test setup with respect to component and/or layout asymmetries is highlighted, while appropriate measures that reduce the CM-to-DM conversion are suggested.

II. FUNDAMENTALS OF THREE-PHASE CM/DM NOISE SEPARATION IN POWER CONVERTERS

A. EMI Noise Equivalent Circuit of a Voltage Source Inverter

Generally, switched-mode converter systems such as a three-phase photovoltaic VSI shown in **Fig. 1** present substantial high frequency spectral components at their AC outputs originating from the Pulse-Width Modulated (PWM) operation of the three half-bridges. Meeting the respective regulations therefore requires suitable EMI filtering, which typically accounts for a considerable amount of the total converter volume, contributes losses and weight and increases the overall cost. Consequently, the aim is to keep the EMI filtering effort as low as possible, which is achieved by a detailed analysis of the converter's EMI noise equivalent circuit. In **Fig. 4 (a)** each of the half-bridges from **Fig. 1** is replaced with two voltage sources \bar{v}_i and $v_{i,\sim}$, $i = \{a', b', c'\}$, representing the

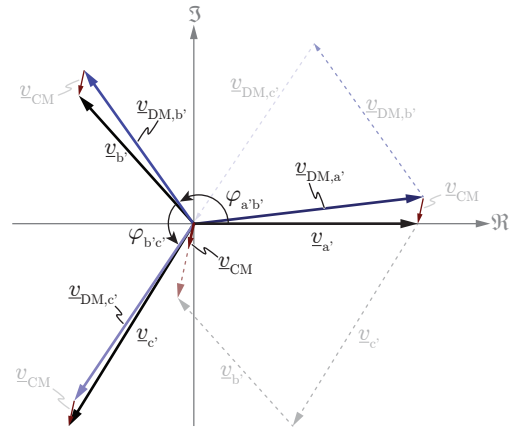


Fig. 5. Phasor diagram showing the decomposition of the three phase voltage components into the respective CM and DM parts.

fundamental frequency component \bar{v}_i (e.g. the 50/60 Hz voltage) and all switching related components $v_{i,\sim}$, respectively. It holds that $v_i = \bar{v}_i + v_{i,\sim}$. A further decomposition is possible by separately considering the CM and DM components of the corresponding phase voltages (cf. **Fig. 4 (b)**) according to

$$v_i = v_{CM} + v_{DM,i}, \quad i = \{a', b', c'\}, \quad (1)$$

where again fundamental and the switching frequency components can be considered separately.

By definition, the CM component is equal in all three phases and can thus be combined to a single voltage source

$$v_{CM} = \frac{v_{a'} + v_{b'} + v_{c'}}{3} \quad (2)$$

with help of the identity

$$v_{DM,a'} + v_{DM,b'} + v_{DM,c'} = 0. \quad (3)$$

It should be noted that this decomposition implicitly assumes equal distribution of the phase impedances and therefore a symmetric distribution of the CM current. In practice, this is typically fulfilled with sufficient accuracy, however, not strictly required [7]. **Appendix A** explains the CM and DM decomposition in a three-phase system in more detail.

The fundamental components are usually not of importance for EMI compliance as they occur far below the relevant regulated frequency range and it is sufficient to consider only the high-frequency switching components (**Fig. 4 (c)**). The inverter dc input midpoint n can be floating with respect to mains ground 0 (protective earth) but there will always be a certain parasitic CM capacitance C_{CM} connecting the two potentials, which in combination with $v_{CM,\sim}$ determines the CM noise. For EMI filter design, the worst-case condition of a short circuit between n and 0 ($v_{n0} = 0$) has to be considered.

Finally, the equivalent circuit of the three half-bridges is simplified to four HF voltage sources, one CM and three DM voltages. Expanding the four HF voltages as a Fourier series results in individual spectral components. For each frequency the corresponding three-phase system composed of the spectral components of the Fourier series of the CM and DM voltages

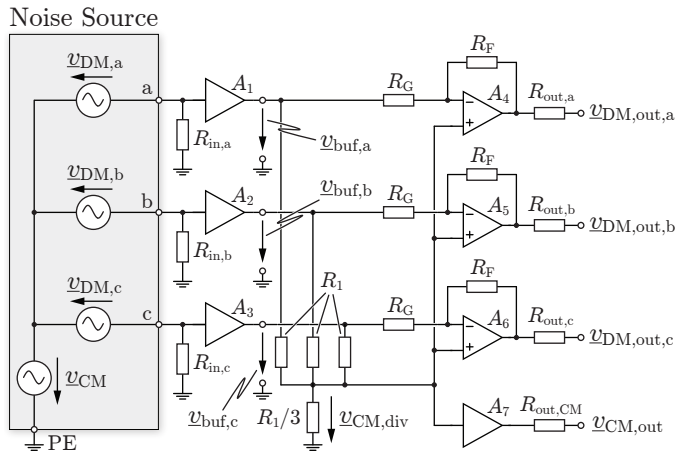


Fig. 6. Schematic drawing of the an active three-phase CM/DM noise separator as described in [4].

can be individually described in a phasor diagram as shown in **Fig. 5** with help of complex phasors \underline{v}_{CM} and $\underline{v}_{DM,i}$, $i = \{a', b', c'\}$. It has to be noted that the 120° phase-shift between the individual phase voltages is given only for the fundamental component and is not necessarily required for the HF voltage components. For better visibility **Fig. 5** still shows phase-shift of around 120° . For simplicity hereinafter \underline{v}_{CM} and $\underline{v}_{DM,i}$ denote complex phasors of the CM and the three DM components of the EMI noise voltage at one specific frequency.

B. Review of Three-Phase CM/DM Noise Separators

The use of a three-phase EMI CM/DM noise separator is required to discuss the CM and DM noise components. Various implementations of three-phase noise separation circuits have been presented in the literature. Most of them are composed of magnetic components and rely on flux superposition/cancellation [3], [6], [8], [9]. Only two variants feature active operational amplifiers [4], [10] where there is no need to match magnetic components. This greatly facilitates handling, operation and the reproducibility. There are alternative implementations using current probes [5] or the separation is simply performed in post-processing [11] given the three individual noise spectra. The latter method is very sensitive to noise and/or measurement errors.

Because a very high performance noise separator is a prerequisite for accurate CM/DM noise decomposition, the most promising approach is the active three-phase CM/DM noise separator proposed in [4], which features a very high reported separation performance. Its schematic is shown in **Fig. 6** including a representation of the HF noise voltage sources at its input ports a , b and c . The input voltages are terminated with $R_{in,i} = 50\Omega$ as required by the standard [12] and are then buffered with amplifiers $A_1 \dots A_3$. With the CM voltage divider composed of three resistors R_1 and resistor $R_1/3$, the CM voltage $\underline{v}_{CM,div}$ is derived according to (2) and is available at the CM output port after buffering with amplifier A_7 . The three DM components are derived from the buffered input

voltages $\underline{v}_{buf,i}$ and the CM voltage based on (1) with three difference amplifiers $A_4 \dots A_6$, i.e.,

$$\underline{v}_{DM,out,i} = \underline{v}_{CM,div} - \underline{v}_{buf,i} \quad (4)$$

The inverted sign of $\underline{v}_{DM,out,i}$ compared to (1) does not influence the measurement, since only the noise voltage magnitudes are relevant for compliance.

To assess the performance of a noise separator it is helpful to consider the Transfer Functions (TF) and Rejection Ratios (RR), which are found by applying either a pure CM ($\underline{v}_{DM,LISN,i} = 0$) or a pure DM ($\underline{v}_{CM,LISN} = 0$) excitation. In the former case, the Common-Mode Transfer Function (CMTF) is defined as the ratio between CM output voltage and CM input voltage

$$CMTF = \left| \frac{\underline{v}_{CM,out}}{\underline{v}_{CM}} \right| \quad (5)$$

Similarly, the Common-Mode Rejection Ratio (CMRR) describes the amount of input CM voltage converted into DM at output port i , i.e.,

$$CMRR_i = \left| \frac{\underline{v}_{DM,out,i}}{\underline{v}_{CM}} \right| \quad (6)$$

For an ideal noise separator the three CMRR responses of the phases are identical.

In the case of a pure DM input the Differential-Mode Transfer Function (DMTF) and the Differential-Mode Rejection Ratio (DMRR) are defined as

$$DMTF_i = \left| \frac{\underline{v}_{DM,out,i}}{\underline{v}_{DM}} \right| \quad (7)$$

and

$$DMRR = \left| \frac{\underline{v}_{CM,out}}{\underline{v}_{DM}} \right| \quad (8)$$

The experimental TF and RR measurements of an active noise separator hardware demonstrator according to [4] are depicted in **Fig. 7** and reveal excellent separation capabilities. A CMRR and DMRR better than -50 dB is reached over almost the entire EMI relevant frequency range, while the CMTF and the DMTF remains very flat. Particularly the performance at elevated frequencies above 1 MHz is significantly better compared to a passive separator (dashed lines in **Fig. 7**, concept of [3]). The deviation of the CMRR and DMRR in **Fig. 7** is caused by parasitic elements such as, e.g., solder joint and Printed Circuit Board (PCB) track resistances. In addition, the measurement setup to assess the CMRR and DMRR includes a residual mismatch. The operation principle and a detailed explanation of the measurement setup are given in [4].

III. THEORETICAL ANALYSIS OF THE INFLUENCE OF AMPLITUDE AND PHASE MISMATCH

The investigation of the active CM/DM noise separator revealed that the symmetry of the PCB layout as well as close matching of parasitic components is of predominant importance. Even small mismatches lead to a significant degradation in the separation capabilities. As illustrated with **Fig. 2**, the CE EMI test setup contains many other elements besides the

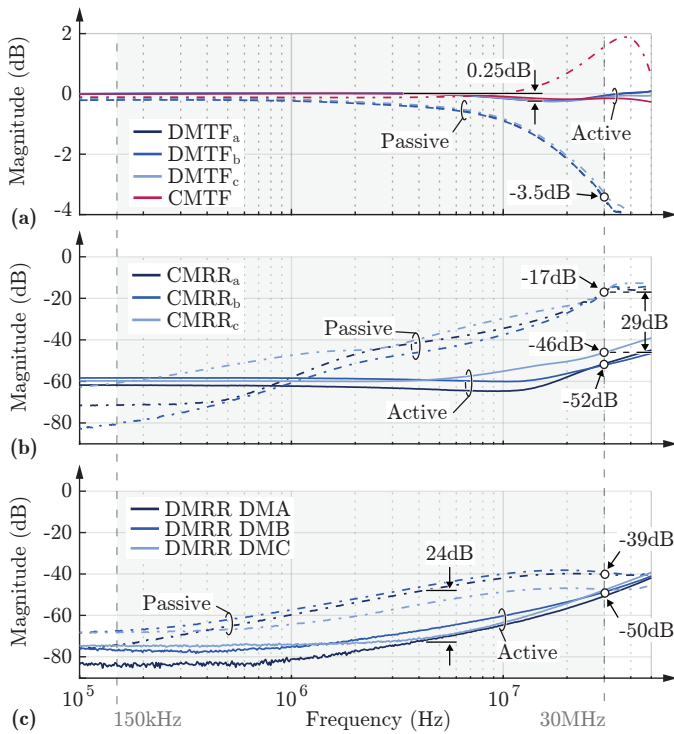


Fig. 7. Transfer functions (TF) and rejection ratios (RR) for the active noise separator of [4] (continuous lines) and the passive separator described in [3] (dashed lines). (a) CMTF and DMTF, (b) CMRR for each DM output and (c) DMRR measured each time with one of the inputs set to zero (DM $_i$ means input i was set to zero).

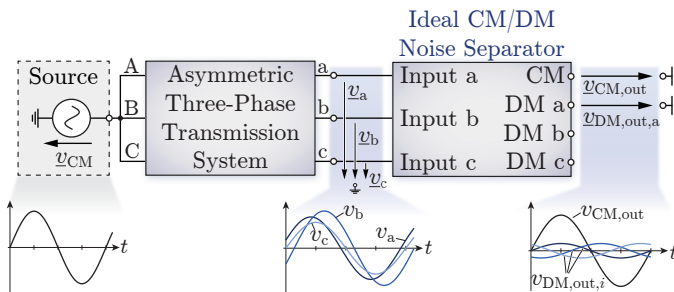


Fig. 8. Schematic representation of amplitude and phase mismatches in an asymmetric three-phase transmission system excited with a pure CM input voltage and the resulting CM-to-DM conversion.

noise separator that could equivalently deteriorate the overall CM/DM separation, since they are responsible for amplitude and/or phase mismatches in a three-phase transmission system (cf. **Fig. 3**). In this section the CM-to-DM conversion for a certain amplitude and/or phase mismatch resulting from an asymmetric three-phase transmission system as indicated in **Fig. 8** is analyzed. In the course of this analysis, the separator itself is assumed ideal, i.e., with infinite CMRR and DMRR as well as perfectly flat CMTF and DMTF, such that the sole impact of external mismatches becomes evident. The amplitude and/or phase mismatches in an asymmetric three-phase transmission system lead to two conceptually identical

phenomena. On the one hand a pure CM input voltage leads to a certain portion of DM components at the output (CM-to-DM conversion, indicated in **Fig. 8**) and on the other hand a pure DM input voltage causes a CM component at the output (DM-to-CM conversion). In **Sections IV to VI** the influence of the elements in a practical EMI test setup according to **Fig. 2** will be experimentally analyzed in detail. For this, a known input signal (either CM or DM) is applied and the corresponding CM and DM voltages are measured using the active noise separator described in the previous section. We restrict the investigation to the case of a CM input and therefore the resulting CM-to-DM conversion for the following reasons:

- i) To perform meaningful experiments it is crucial to apply pure CM or DM input signals to the system. The generation of three input voltages perfectly equal in amplitude and phase (pure CM input) is much easier to realize with high accuracy compared to a well-balanced three-phase DM voltage system. Yet, the latter would indeed be possible e.g. with a very fast FPGA that generates the three 120° phase-shifted DM voltage components. In order to measure CM-to-DM conversions in the range of -60 dB, this would require a time resolution in the sub-nanosecond range as shown in [4], which is very challenging to achieve in practice.
- ii) For a given amplitude or phase mismatch it was found that the worst-case CM-to-DM conversion is more pronounced compared to the reciprocal DM-to-CM conversion. Comparison plots for verification can be found in **Appendix B**.
- iii) The exact CM noise source in a power converter is usually very difficult to predict in practice. Therefore, accurate measurements for this case are very valuable.

The remainder of this section theoretically analyzes the CM-to-DM conversion as a result of a general amplitude and/or phase mismatch.

A. Amplitude Mismatch

Given are three nominally identical sinusoidal test voltages $v_a(t)$, $v_b(t)$ and $v_c(t)$ for channels a , b and c without phase-shift but different amplitudes V_a , V_b and V_c (cf. **Fig. 9 (a)**). With voltage a as reference, two relative amplitude mismatches V_b/V_a and V_c/V_a result. The amplitude mismatches lead to a CM-to-DM conversion. An idealized CM/DM separation according to (1) and (2) reveals the CM-to-DM component i conversion (CMDM $_i$) as

$$\text{CMDM}_a = \frac{V_{\text{DM},a}}{V_{\text{CM},\text{out}}} = \frac{2 - V_b/V_a - V_c/V_a}{1 + V_b/V_a + V_c/V_a} \quad (9)$$

$$\text{CMDM}_b = \frac{V_{\text{DM},b}}{V_{\text{CM},\text{out}}} = \frac{2 \cdot V_b/V_a - 1 - V_c/V_a}{1 + V_b/V_a + V_c/V_a} \quad (10)$$

$$\text{CMDM}_c = \frac{V_{\text{DM},c}}{V_{\text{CM},\text{out}}} = \frac{2 \cdot V_c/V_a - 1 - V_b/V_a}{1 + V_b/V_a + V_c/V_a} \quad (11)$$

The CM-to-DM conversion is normalized with respect to the CMTF (5), i.e., the CM-to-DM conversion is the ratio of the voltage amplitude $V_{\text{DM},i}$ of DM component i divided by $V_{\text{CM},\text{out}}$. The conversion to DM components a and b (CMDM $_a$ and CMDM $_b$) for varying amplitude ratios V_b/V_a and V_c/V_a

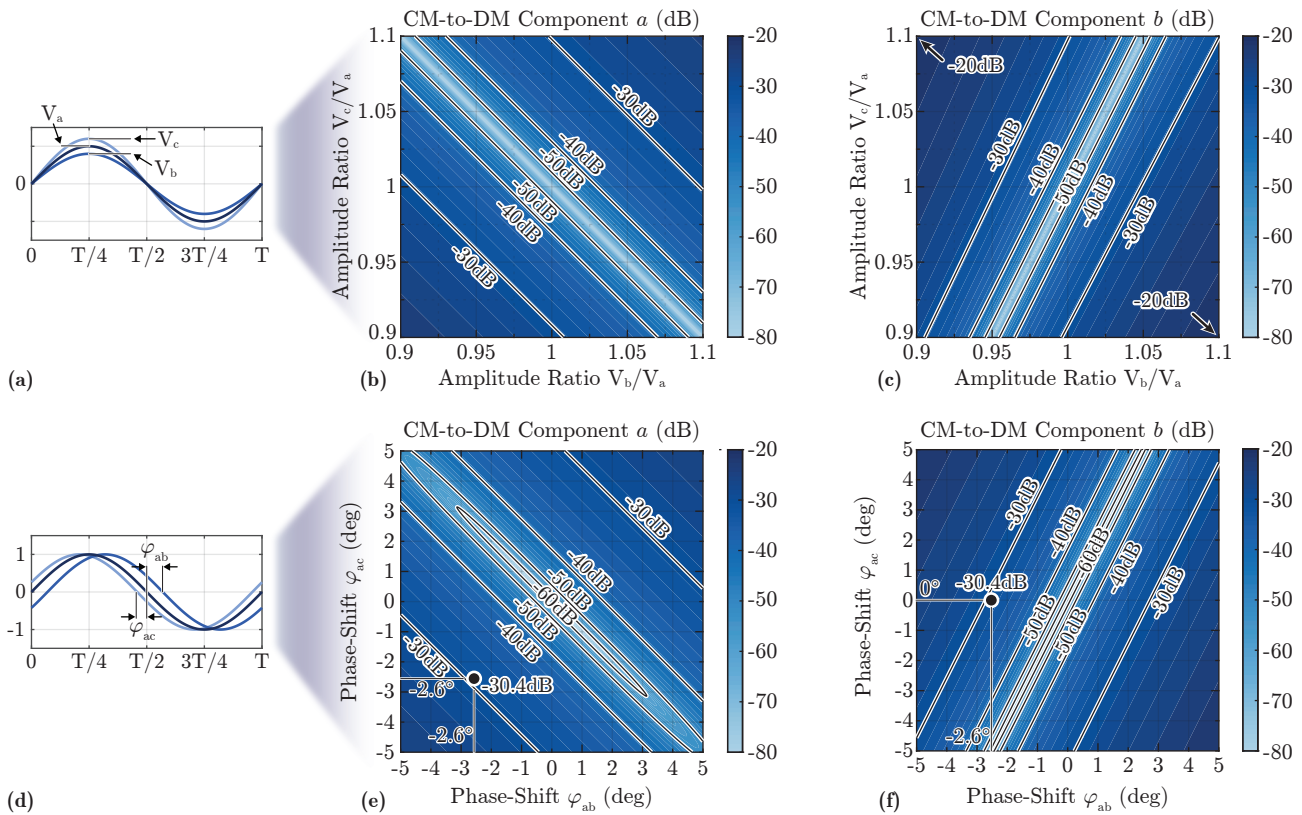


Fig. 9. Amplitude and phase mismatches at the output of an unsymmetric three-phase transmission system and related characterization with a CM-to-DM conversion. Input channel a is treated as reference and input voltages b and c show amplitude/phase mismatches with respect to voltage a . (a)-(c) Considering only an amplitude mismatch V_b/V_a and V_c/V_a and (d)-(f) considering only a phase mismatch φ_{ab} and φ_{ac} .

is depicted in **Fig. 9 (b)-(c)**, respectively. From (10) and (11) follows that the result for DM component c looks identical to the one for component b when the two amplitude ratio axes are flipped. In contrast, the result for the DM component a looks different, because input a is treated as reference channel. The CMDM_a is zero (minus infinity in dB) for $V_b/V_a + V_c/V_a = 2$, since the two mismatches cancel each other out perfectly. In the same way, for $2 \cdot V_b/V_a - V_c/V_a = 1$ there is no conversion from CM to DM component b . It is clearly visible, that an amplitude mismatch of only $\pm 10\%$ can result in a CM-to-DM conversion up to -20 dB (indicated in **Fig. 9 (c)**).

B. Phase Mismatch

Similarly to an amplitude mismatch, the influence of a phase mismatch between three nominally identical test voltages $v_a(t)$, $v_b(t)$ and $v_c(t)$ (cf. **Fig. 9 (d)**) on the CM-to-DM conversion for DM components a and b is shown in **Fig. 9 (e)-(f)**, again normalized with respect to the CMTF. Further, v_a is treated as reference voltage, i.e., v_b and v_c have a phase-shift of $\varphi_{ab} = \varphi_b - \varphi_a$ and $\varphi_{ac} = \varphi_c - \varphi_a$, respectively, with respect to v_a . When flipping the phase mismatch axes in **Fig. 9 (f)**, the conversion from CM to DM component c results. It becomes clear that even small phase mismatches are related to a significant CM-to-DM conversion. Only in a very narrow range the corresponding phase mismatches cancel each other.

C. Combined Amplitude and Phase Mismatch

The analyses in the previous two subsections refer to cases where either only amplitude or only phase mismatches are present. In practice, usually both occur at the same time. For the high-frequency EMI noise analysis the three phase voltages are generally independent from each other meaning that the CM-to-DM conversion depends on four parameters (V_b/V_a , V_c/V_a , φ_{ab} and φ_{ac}). To reduce the complexity to two parameters, the two amplitude as well as the two phase mismatches are combined to two parameters e_V and φ . For each combination of phase mismatch φ and amplitude mismatch e_V **Fig. 10** shows the related worst-case CM-to-DM conversion for all possible combinations of phase-shifts $\{\varphi_{ab}, \varphi_{ac}\} \in [-\varphi, \varphi]$ and amplitude mismatches $\{V_b/V_a, V_c/V_a\} \in [1/e_V, e_V]$ of test voltages v_a , v_b and v_c . The conversion from CM to DM component a (**Fig. 10 (a)**) and b (**Fig. 10 (b)**) are depicted. The conversion to DM component c is identical to DM component b because only the worst-case of all possible mismatch combinations is considered. For the same reason the surfaces in **Fig. 10** are monotonically increasing with increasing φ and e_V . The slightly different appearance of the surfaces for DM output a and b is due to the choice of channel a as reference. The CM-to-DM conversion is normalized with respect to the CMTF (5) and the plots in **Fig. 10** therefore illustrate the CM-to-DM conversion relative to the actual CMTF. This will facilitate the comparison with actual measurements as will be

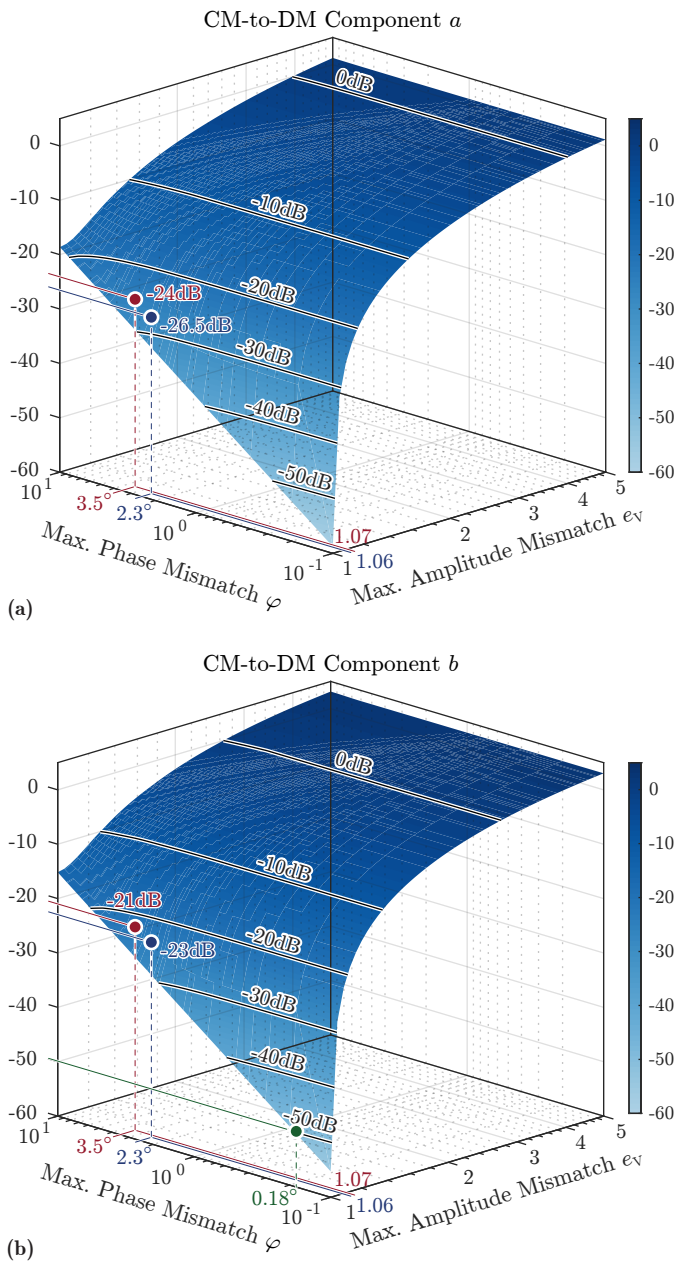


Fig. 10. Worst-case CM-to-DM conversions for DM component *a* (a) and *b* (b) considering all possible combinations of amplitude mismatches $\{V_b/V_a, V_c/V_a\} \in [1/e_V, e_V]$ and phase mismatches $\{\varphi_{ab}, \varphi_{ac}\} \in [-\varphi, \varphi]$ of inputs *b* and *c* assuming again input *a* as reference.

seen later.

Based on the theoretical calculations, the CM-to-DM conversion resulting from various sources of mismatch and asymmetry can be estimated based on the expected amplitude and/or phase mismatch. In the following sections, the most prominent effects are analyzed and experimentally verified.

IV. MISMATCHED THREE-PHASE CONNECTIONS

In a first step, the impact of cables with unequal length for the connection of the EUT, LISN and noise separator is analyzed. In **Fig. 11** the provided measurement setup is

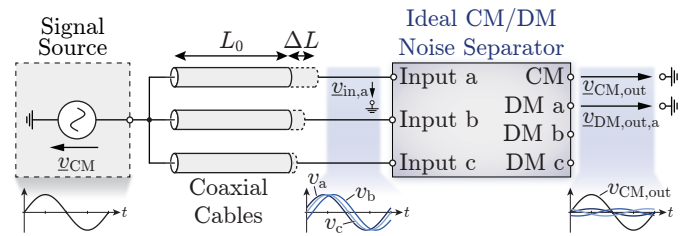


Fig. 11. Schematic representation of the CM-to-DM conversion introduced by connection cables with unequal length.

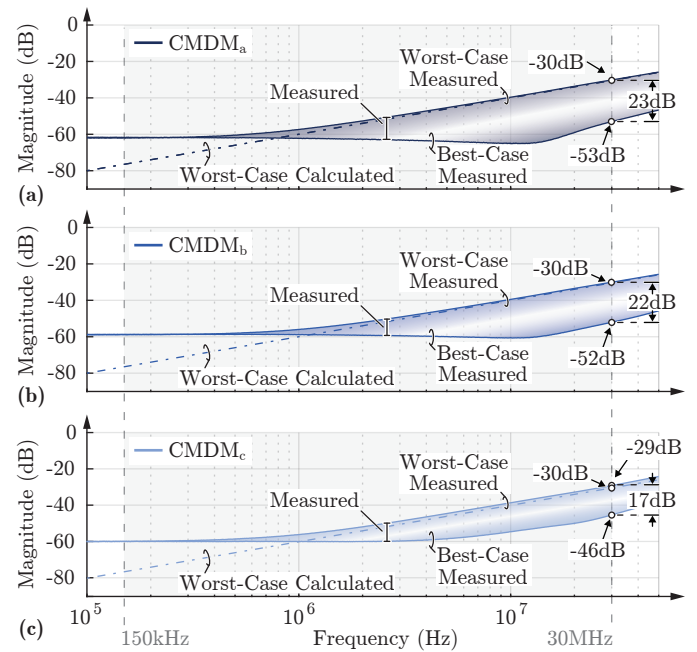


Fig. 12. Best- and worst-case CM-to-DM conversion measurements for all possible combinations of a cable mismatch at the noise separator inputs ($L_0 = 22$ cm nominal cable length, length mismatch $\Delta L = 4.8$ cm). The calculated CM-to-DM conversion assuming an ideal noise separator is included for the worst-case length-mismatch configuration for each channel (dashed lines).

shown, where a network analyzer [13] is used to apply a CM input voltage to the active noise separator and to measure the respective output voltages. The CM voltage u_{CM} is connected to the noise separator inputs with three coaxial cables ($Z_0 = 50 \Omega$, [14]) of nominal length L_0 and selectively added pieces with additional length ΔL . Due to the three slightly phase-shifted signals at the separator inputs, a certain DM portion besides the CM component results at the separator output. **Fig. 12** shows the measurement results for a practically relevant case with short $L_0 = 22$ cm cables and an additional piece with length $\Delta L = 4.8$ cm realized with two BNC adapters (male-male and female-female connected together). All possible combinations of adding a length mismatch ΔL to any of the cables are measured. For each DM output the corresponding best- and worst-case measurement result is plotted (shaded area). All other variants yield results in between the two extreme cases. It has to be noted, that the

measurements in **Fig. 12** are obtained with the active noise separator according to **Figures 6 and 7** and therefore the separator CMRR could slightly influence the measurements. The dashed line represents the worst-case calculated CM-to-DM conversion for all considered length mismatches.

As expected, the respective best-case measurements occur when the cables of all channels have the same length L_0 or $L_0 + \Delta L$. The results then closely match with the separator's inherent CMRR depicted in **Fig. 7**, which proves that the absolute phase-shift has no influence on the CM-to-DM conversion but only the relative phase mismatch between the channels matters. In all channels the worst-case measurement closely matches the corresponding theoretical value in the frequency range above 1 MHz where the separator's inherent CMRR is much better compared to the CM-to-DM conversion resulting from the cable length mismatch.

The utilized coaxial cables show a very low insertion loss at the given frequency range (< 0.1 dB/m [14]) and therefore the amplitude is barely altered by the cable length mismatch. There is, however, a phase-shift

$$\Delta\varphi(f) = \omega \cdot \Delta t = 2\pi \cdot f \cdot \Delta t \quad (12)$$

linearly dependent on frequency f and time difference Δt (skew) between two signals. The latter is given by

$$\Delta t = \Delta L / v_{\text{cable}}, \quad (13)$$

with the cable length mismatch ΔL and signal propagation speed v_{cable} . For the employed RG-58 coaxial cables [14] with $v_{\text{cable}} \approx 0.66 \cdot c = 2 \cdot 10^8$ m/s a length mismatch $\Delta L = 4.8$ cm leads to a phase-shift $\Delta\varphi \approx 2.6^\circ$ at 30 MHz. The measurements of the worst-case in CM-to-DM conversion at 30 MHz in **Fig. 12** (-30 dB) coincide with the theoretical considerations visualized **Fig. 9 (e)-(f)** where the points corresponding to the respective worst-case ($\varphi_{ab} = \varphi_{ac} = -2.6^\circ$ for channel a and $\varphi_{ab} = -2.6^\circ$; $\varphi_{ac} = 0^\circ$ for channel b) are highlighted. The results clearly show, that the connecting cables must be chosen with equal length. The separator itself achieves a CMRR of around -50 dB at 30 MHz, and in order to be not limited by the cable mismatch, the external CM-to-DM conversion must be better than -50 dB. This is achieved if it is ensured that the phase-shift is kept smaller than 0.18° (considering no amplitude mismatch, $e_V = 1$) according to **Fig. 10 (b)** (indicated with the green marker). Accordingly, using (12) and (13) the cable mismatch ΔL must be lower than 3.3 mm. This clearly points out the importance of length-matched cables within the whole EMI test setup (power cables from the EUT to the LISN, coaxial cables from the LISN to the noise separator and from the noise separator to the test receiver).

Remark:

For the given case, only the length mismatch is considered as an influencing factor on the signal propagation time. However, a mismatch of the coaxial cable characteristic impedance could manifest itself in a slightly different signal propagation speed v_{cable} and thus also in a different propagation time. With the employed RG-58 coaxial cables, the measured CM-to-DM conversion matches very well with the calculated value obtained with the datasheet value of the signal propagation

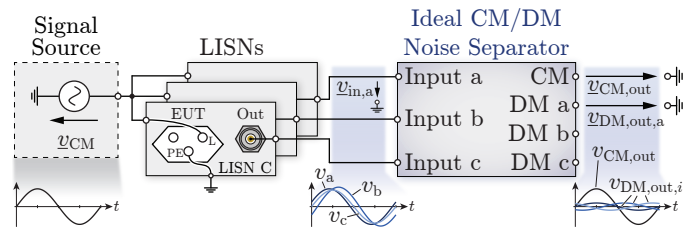


Fig. 13. Schematic representation of the CM-to-DM conversion introduced by asymmetries between the individual LISNs resulting in a certain DM portion besides the desired CM component at the separator outputs.

speed. Therefore, the assumption of a constant characteristic impedance $Z_0 = 50 \Omega$ is sufficient in this case. Reflection coefficient measurements with the 22 cm BNC coaxial cable alone and the cable including the two BNC adapters, both terminated with the same 50Ω load, show a change of less than 0.1Ω in the characteristic impedance at 30 MHz between the two cases. For frequencies below some MHz hardly any effect is noticeable. With this same argumentation the realization of the length mismatch with BNC adapter pieces is justified.

V. ASYMMETRIES IN THE LISN

A. Conventional LISN Measurement

To perform the noise separation, all three LISN output voltages must be measured at the same time. Since most three-phase LISNs do not support concurrent measurements of all three phases, in practice three single-phase LISNs have to be used. They have to be designed according to the CISPR 16-1-2 standard [2] with an EUT port input impedance $\underline{Z}_{\text{EUT}}$ of nominally $50\Omega || 50 \mu\text{H}$ and a maximum magnitude deviation of $\pm 20\%$ and phase deviation of $\pm 11.5^\circ$ (cf. **Fig. 20** in **Appendix C**). A mismatch of $\underline{Z}_{\text{EUT}}$ results in a mismatch of the TF from EUT input port to HF measurement output port, which means that for a pure CM input voltage at the EUT ports the measured HF output port voltages show an amplitude and phase mismatch. Fortunately, commercial LISNs show considerably tighter specifications than required by the standard. Particularly devices of the same type are very closely matched. Nevertheless, the influence of the residual asymmetry on the separation performance has to be analyzed in detail. **Fig. 13** shows the basic measurement setup used to evaluate the influence of LISN mismatches on the separation capability and schematically shows the aforementioned effect of CM-to-DM conversion. As mentioned in the beginning, three single-phase LISNs are utilized to allow a simultaneous measurement of all three phases. An advantage of using three single-phase LISNs is the superior shielding and isolation between the three measurement channels thanks to the individual enclosure of each LISN. This helps to suppress undesired cross-couplings between the three phases. In **Fig. 14 (a)** the TFs from EUT input to HF output for the three employed single-phase LISNs (Rohde & Schwarz ENV-216 [15]) are depicted (continuous lines: magnitude; dashed lines: phase). From the three TFs the calculated relative amplitude mismatch $e_{V,ab}$ and $e_{V,ac}$ and phase mismatch φ_{ab} and φ_{ac} is shown

in **Fig. 14 (b)** and **(c)**. The measurements distinctly verify the close matching of the three LISNs but also reveal that even if the devices are the same model and type, there are still certain residual mismatches due to e.g. internal component or assembly tolerances, in particular at high frequencies. It has to be noted that the pronounced high-pass behavior below 200 kHz results from the $50\ \Omega$ inner resistance of the network analyzer's generator port together with the EUT port input impedance and is not inherent to the LISN itself. This effect could be calibrated out but since the amplitude and phase mismatches in this region are anyway very small, this is omitted here.

The illustrated measurements represent a practically relevant case, where two LISNs (*a* and *b*) were acquired at the same time whereas the third one (*c*) was obtained at a later date. Due to manufacturer side hardware revisions and improvements, the internal construction of the newer device may not be identical to the older ones. This becomes evident in **Fig. 14 (a)-(c)** where LISN *c* shows a slightly different transfer behavior, which manifests itself in a more pronounced amplitude and phase mismatch $e_{V,ac} = V_{in,c}/V_{in,a}$ and $\varphi_{ac} = \varphi_c - \varphi_a$ at distinct frequencies with respect to reference LISN *a*.

Based on the measured LISN transfer functions the CM-to-DM conversions to all DM output ports are calculated at each frequency individually under the assumption of an ideal separator (dashed lines in **Fig. 14 (d)**). Furthermore, the CM-to-DM conversions were measured using the active noise separator and are plotted in **Fig. 14 (d)** as well. It is seen that the measurement results are slightly worse than the calculated ones. There are multiple reasons for this such as the influence of the separator CMRR as well as possible coupling effects due to the connection of all three LISNs at the same time to the CM input. Those effects are not treated in the transfer function based calculation of the CM-to-DM conversion. It has to be noted that the plotted CM-to-DM conversions are already normalized with respect to the desired CMTF (5), i.e., the average of the three LISN transfer functions $LISN_{a,b,c}$.

With the maximum amplitude mismatch e_V of 1.07 and the maximum phase mismatch $\varphi = 3.52^\circ$, the worst-case CM-to-DM conversion according to **Fig. 10** would be estimated as $-24\ \text{dB}$ for $CMDM_a$ and $-21\ \text{dB}$ for $CMDM_b$ and $CMDM_c$ (indicated with red markers). The calculated results in **Fig. 14 (d)** are slightly better because the given combination of $e_{V,ab}$, $e_{V,ac}$, φ_{ab} and φ_{ac} does not represent the worst-case as depicted in **Fig. 10**, whereas the measured value becomes as low as $-20.9\ \text{dB}$ at $21.7\ \text{MHz}$. It has to be noted that in this particular case the estimation of the worst-case CM-to-DM conversion with help of **Fig. 10** using the worst-case amplitude and phase mismatches over the whole frequency range according to **Fig. 14** gives an over-pessimistic value because the three LISNs are closely matched over a wide frequency range and show considerable mismatches only at distinct frequencies.

In comparison with the performance of the separator itself (cf. **Fig. 7**), a significant degradation in the separation capabilities (around $20\ \text{dB}$ or a factor of 10 at elevated frequencies) is observed. At some frequencies, however, the performance with the LISNs is – contrary to intuition – better than the

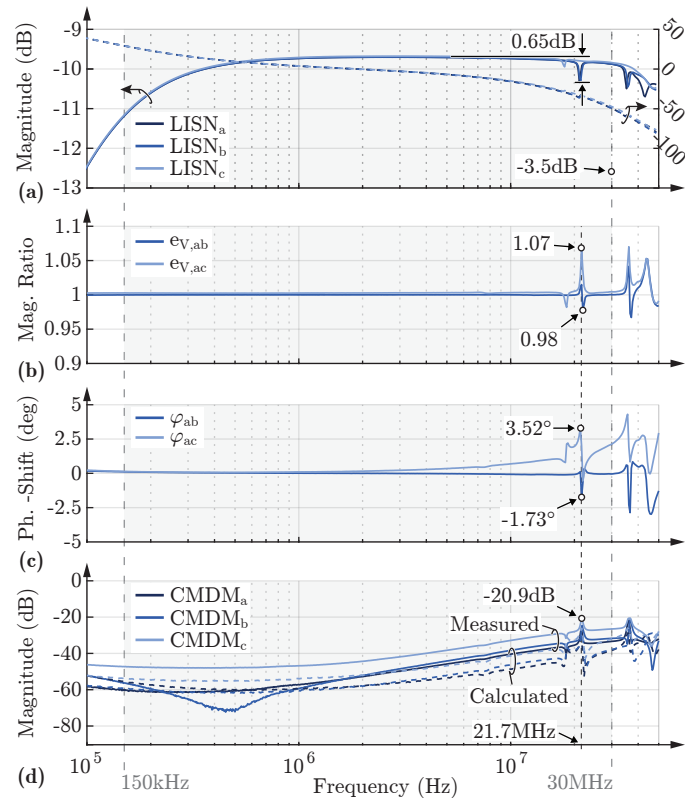


Fig. 14. (a) Transfer functions of the three single-phase LISNs (continuous: magnitude; dashed: phase), (b) the resultant calculated amplitude mismatches $e_{V,ab} = V_{in,b}/V_{in,a}$ and $e_{V,ac} = V_{in,c}/V_{in,a}$ and (c) the phase mismatches φ_{ab} and φ_{ac} ; (d) shows the measured CM-to-DM conversions for each DM output channel including the finite CMRR of the noise separator (continuous lines) as well as the calculated CM-to-DM conversions assuming an ideally performing noise separator (dashed lines).

performance of the noise separator alone. The reason is that external mismatches can counteract an internal mismatch from the separator and therefore improve the overall performance. In conclusion, it is generally inevitable to use LISNs of the exact same type and manufacturer and ideally from the same hardware revision to minimize the resulting imbalances.

B. External High-Frequency Measurement

In a simplified form, the LISN HF measurement path can be described as first-order High-Pass Filter (HPF) formed by C_{HP} (cf. **Fig. 2**) and the $50\ \Omega$ termination. The high-pass behavior is required to attenuate any LF voltage ($50/60\ \text{Hz}$ fundamental components) that would otherwise saturate or even destroy the connected measurement equipment. With an external HPF connected at the EUT port (and with non-terminated LISN HF measurement port) to measure the EMI noise as shown in **Fig. 15 (a)**, potentially a closer matching can be achieved, since the LISN's internal measurement path is omitted. A certain influence of the slightly mismatched Z_{EUT} remains, since the signal source still sees a part of Z_{EUT} but the effect is less severe as verified with the CM-to-DM conversion

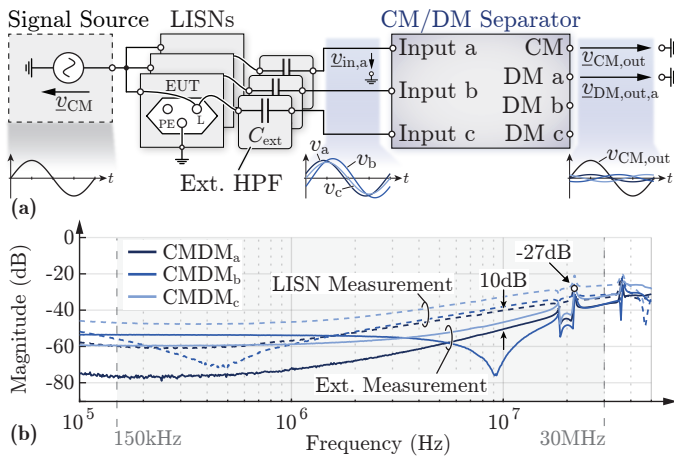


Fig. 15. (a) Extension of the LISN test setup with three external high-pass filters (C_{ext} together with separator input impedance) and (b) the resulting CM-to-DM conversion (continuous lines) in comparison with the direct LISN measurement (dashed lines) as presented before.

measurements depicted in **Fig. 15 (b)**, again normalized with respect to the desired CMTF. The dashed lines correspond to the measurement with the LISN as seen in **Fig. 14 (d)**, whereas the continuous lines denote measurements with an external HPF, i.e., three matched external capacitors C_{ext} with a value of 140 nF each in conjunction with the closely matched $50\ \Omega$ separator input impedance (cut-off frequency $f_{c,\text{HPF}} \approx 23\ \text{kHz}$). Throughout almost the entire relevant frequency range a lower CM-to-DM conversion is achieved with an improvement of at least 10 dB at 10 MHz and 6 dB ($-27\ \text{dB}$ in contrast to $-21\ \text{dB}$, cf. **Fig. 14 (d)**) at the worst-case frequency of 21.7 MHz. For low frequencies the cancellation of error contributions of the separator itself and the external mismatches is very evident, particularly for channel *a*. It has to be noted that for $f > f_{c,\text{HPF}}$ the impedance seen by the EUT is primarily given by the $50\ \Omega$ input resistance of the noise separator. Therefore, in the frequency range of interest from an impedance point of view it does not matter whether the LISN's internal measurement path or the external HPF is used. This is further justified in **Appendix C** that shows the simulated $\underline{Z}_{\text{EUT}}$ for both cases together with the CISPR 16-1-2 limits.

Remark:

Some LISNs feature a more complex HF measurement path with higher order HPFs including capacitive and inductive filter elements [15]. This makes close matching even more difficult. Therefore, in the interest of high symmetry, a first-order HPF is clearly favorable. Additional closely matched $50\ \Omega$ attenuators can be inserted between the external HPF and the noise separator inputs to ensure sufficient attenuation of the LF voltage components, if required.

VI. THREE-PHASE EMI FILTER

The primary goal of precise EMI CM/DM noise separation is the identification and adjustment of insufficiently performing EMI filters in case of exceeding the limiting values. Fur-

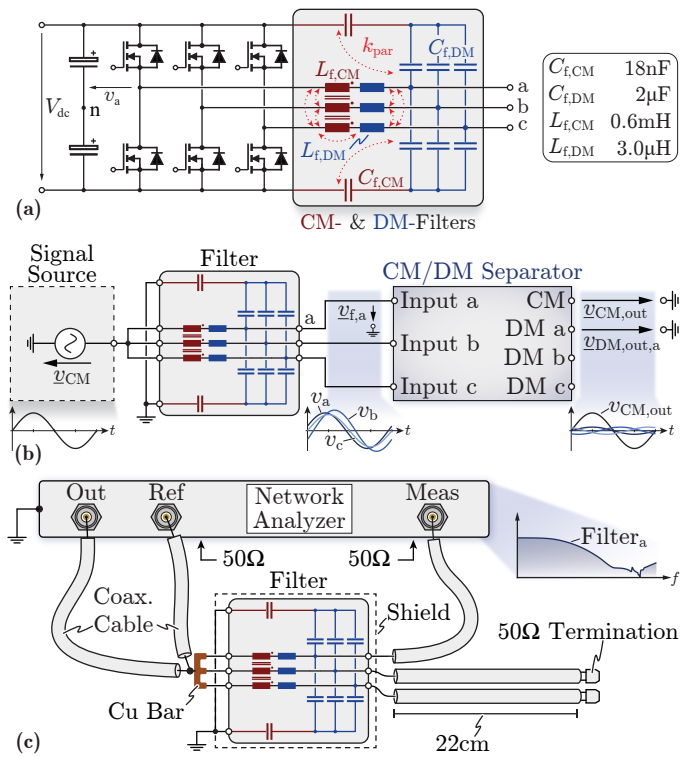


Fig. 16. (a) Three-phase inverter with a single-stage CM/DM output filter, where the components highlighted in red are solely responsible for CM filtering whereas the blue elements are primarily effective for DM filtering. (b) configuration to measure the filter CM transfer function and the CM-to-DM conversion. (c) measurement setup to characterize the individual phase filter transfer functions with a network analyzer.

thermore, the measured noise voltages can be compared with expected values obtained from calculations or simulations. The corresponding models can then be adapted and improved. Provided there is a setup with very closely matched connections and highly symmetric LISNs, a very critical part for accurate splitting of CM and DM EMI noise is the EMI filter itself. Even a very simple filter structure such as the single-stage second order inverter output filter shown in **Fig. 16 (a)** can be responsible for the conversion of CM to DM noise and vice versa due to e.g. mismatches of the parasitic elements and the PCB layout or unwanted couplings k_{par} of magnetic and capacitive elements within a phase and also between the phases [16], [17]. The filter in **Fig. 16 (a)** is a combined CM and DM filter with dedicated components for DM filtering (blue) and CM filtering (red and blue). Typically, the CM inductance $L_{f,\text{CM}}$ realized on a high permeability core is much larger than the DM filter inductance $L_{f,\text{DM}}$, which could be solely the stray inductance of the CM inductor. Therefore, the CM capacitance $C_{f,\text{CM}}$ is considerably smaller compared to the DM capacitance $C_{f,\text{DM}}$, assuming comparable attenuation requirements for CM and DM components (similar filter cut-off frequency). This particular single-stage filter is designed for a nominal CM attenuation of around $-35\ \text{dB}$ at the inverter switching frequency $f_{\text{sw}} = 350\ \text{kHz}$.

In **Fig. 16 (b)** the filter evaluation measurement setup for

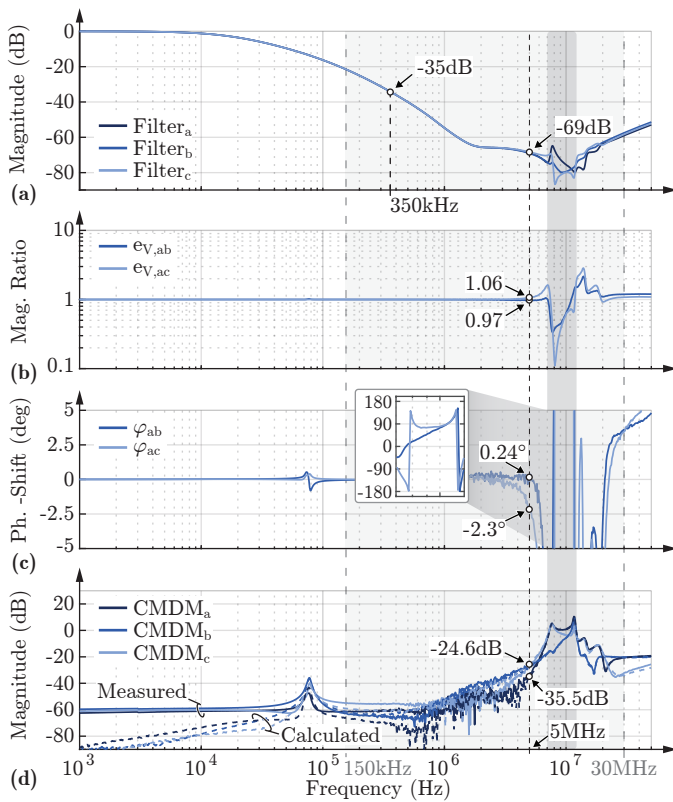


Fig. 17. (a) Measured filter CM transfer functions and therefrom (b) the calculated amplitude mismatches $e_{V,ab}$ and $e_{V,ac}$ and (c) the calculated phase mismatches φ_{ab} and φ_{ac} ; (d) calculated CM-to-DM conversion based on the amplitude and phase mismatches as well as the CM-to-DM conversion measured using an active three-phase noise separator.

a pure CM excitation is shown. The three inputs of the filter are excited simultaneously with a CM voltage source and the dc link terminals are both shorted to ground. The filter TFs $\text{Filt}_i = v_{f,i}/v_{\text{CM}}$ from CM input to filter output i ($i \in \{a, b, c\}$) are measured using a network analyzer in a direct measurement configuration without the noise separator (cf. Fig. 16 (c)). They are depicted in Fig. 17 (a) together with the calculated relative amplitude and phase mismatches e_V and φ (Fig. 17 (b)-(c)). Finally, Fig. 17 (d) shows the calculated CM-to-DM conversion based on the measured filter TFs under the assumption of an ideal noise separator (dashed lines) together with the measured CM-to-DM conversion using the active noise separator (continuous lines). Both are normalized with respect to the (desired) filter CMTF. Hence, a CM-to-DM conversion of e.g. -20 dB means, that for a pure CM input the output voltage measured at the separator's DM output port is ten times lower than the one measured at the CM output port. Because the calculated CM-to-DM conversion is obtained with phase sensitive additions and subtractions, it is very prone to measurement errors and therefore the filter TFs must be measured with the highest possible accuracy. In addition, the desired CM transfer function itself already shows significant attenuation at high frequencies and the CM-to-DM conversion is expected to be even lower (i.e. the

normalized CM-to-DM conversion should be lower than 0 dB). To achieve accurate results for the case at hand, the filter is shielded with metal plates, the applied CM input voltage is measured directly at the filter input terminals (reference measurement cf. Fig. 16 (c)) and it is ensured that all outputs are connected with equally long cables and are terminated with 50Ω . The 50Ω terminations prevent potential reflections in the coaxial cables used to connect the network analyzer and ensures equal filter loading for all measurement scenarios. The usage of a 50Ω termination impedance is typically found in practical applications as most measurement devices expect a 50Ω environment. Moreover, it is a de facto standard scenario that allows to compare different measurements. Finally, the LISN EUT ports feature an impedance close to 50Ω over the specified frequency range (cf. Appendix C), which further justifies the measurement in a 50Ω environment. It has to be said, however, that there is a fundamental uncertainty whether the obtained performance measured with a certain test setup corresponds to the achieved performance in a practical setup.

Fig. 17 shows that the three channels are matched very closely up to 2 MHz resulting in a normalized CM-to-DM conversion of no more than -40 dB. At 2 MHz the desired CM attenuation of the filter is as low as -65 dB, which means the residual voltage at the DM output ports is attenuated by -105 dB (a factor of 177000) with respect to the applied CM input voltage. This illustrates the high required measurement dynamic range. The measured CM-to-DM conversion conforms very well with the calculated one, particularly in the relevant frequency range for CE. Only for frequencies below 50 kHz the active separator limits the performance due to its finite CMRR. As an example, the maximum magnitude mismatches $e_{V,ab} = 0.24^\circ$ and $e_{V,ac} = 1.06$ and phase mismatches $\varphi_{ab} = 0.97$ and $\varphi_{ac} = -2.3^\circ$ are indicated in Fig. 17 at $f = 5$ MHz to allow a comparison of the measured CM-to-DM conversion with the theoretically expected worst-case values. In the diagram of Fig. 10 the corresponding point with $e_V = \max\{e_{V,ab}, e_{V,ac}\} = 1.06$ and $\varphi = \max\{\varphi_{ab}, \varphi_{ac}\} = -2.3^\circ$ is indicated with blue markers. The measured CM-to-DM conversions of -35.5 dB for channel a and -24.6 dB for channels b and c are slightly better than the predicted worst-case values of -26.5 dB and -23 dB, respectively. Again, this is because the relative filter amplitude and phase mismatches at $f = 5$ MHz do not correspond to the worst-case of all possible mismatch combinations $e_{V,ab}$, $e_{V,ac}$, φ_{ab} and φ_{ac} in the range of $[1/e_V, e_V]$ and $[-\varphi, \varphi]$.

The CM-to-DM conversion is attributed to filter asymmetries with very high confidence, given the very high performing noise separator together with the carefully matched measurement setup. In the frequency range between 7 and 12 MHz (highlighted in gray) the normalized CM-to-DM conversion is greater than 0 dB, meaning that even for a pure CM filter input voltage, the DM components of the output voltages have a larger magnitude compared to the CM component. At high frequencies this is of particular concern because the desired CM filter attenuation is very strong, i.e., the CM output signal is very small, but at the same time mismatches are typically more pronounced. Possible examples are the large phase mismatch (zoomed out view in Fig. 17 (c)) and the impact

of unwanted couplings k_{par} attributed to parasitic elements of the employed filter components and the PCB layout. A very important note is that the typically employed layout of a three-phase EMI filter consists of three identical filter cells (one for each phase) placed next to each other on a PCB. This arrangement has an inherent asymmetry, since the middle cell is surrounded by two other filter cells whereas the outer cells are on one side either close to a (shielding) enclosure or other components. This inherent asymmetry also remains if the three-phase EMI filter is shielded but is minimized if the shield is placed with a sufficient distance as it is done in this work. Generally, a certain mismatch can always be attributed to geometry and not only to component and layout tolerances.

The measurements manifestly show that a high performance noise separator can not only be used to identify CM and DM components in the total EMI noise spectrum but also helps to reveal filter asymmetries. In contrast to consecutive measurements of the three filter TFs and the calculation of the CM-to-DM conversion, the direct measurement is more robust, since potential repeatability errors of the network analyzer and small changes in the setup and/or the surrounding have no influence on the measurement as all three channels are measured concurrently.

It is evident that for a normalized filter CM-to-DM conversion approaching 0 dB, no statement regarding the origin of the CE (CM or DM) can be made by simply looking at the measured separator output voltages, even if both, the separator and the whole EMI test setup are perfectly symmetric. Therefore, from an EMI characterization point of view, a symmetric filter construction and layout is extremely important and should be taken into consideration as a design criterion together with more prominent measures like overall size, losses, weight and cost. As a further benefit, careful filter design and layout allows to reduce the typically included attenuation margins, since the real filter behavior matches more closely with the simulated behavior. This in turn reduces the overall filter size.

VII. CONCLUSION

The decomposition of the total EMI noise into its Common-Mode (CM) and Differential-Mode (DM) part is a useful tool for power electronics engineers, who want to design/commission a converter that complies with Conducted Emissions (CE) regulations. A noise separator is used in order to realize the CM/DM EMI noise decomposition. Typically, a high performance of the CM/DM noise separator, characterized by a high Common-Mode Rejection Ratio (CMRR) and Differential-Mode Rejection Ratio (DMRR), is required. However, this is not sufficient. It is shown in this paper that even with an ideally performing noise separator (infinite CMRR and DMRR), the results can be ambiguous due to nonidealities in the test setup. It is deduced that the nonidealities mainly originate from asymmetries in the connection cables, the Line Impedance Stabilization Network (LISN) and the EMI filter of the converter. The nonidealities of the test setup result in an unwanted conversion of CM into DM and vice versa. For example, if the Equipment Under Test (EUT) generates purely CM noise, a CM-to-DM noise conversion occurs due

to asymmetries in the test setup, before the EMI noise is processed by the separator.

This paper quantitatively characterizes the CM-to-DM noise conversion (and not the reciprocal DM-to-CM noise conversion) because:

- i) The application of a pure CM signal to all inputs for testing purposes is much more convenient compared to three perfectly 120° phase-shifted DM signals.
- ii) For a given mismatch the CM-to-DM conversion is typically more pronounced compared to the contrary DM-to-CM conversion.
- iii) The CM noise is the main concern on converter CE compliance at high frequencies.

Three identical voltages at the separator input would be expected in case of a pure CM noise source and an ideal test setup. In reality, three marginally different voltages appear at the separator input due to the nonidealities of the setup. Namely, the three input voltages exhibit a phase mismatch φ and/or an amplitude mismatch e_v . In a first step, a theoretical analysis is performed, where the CM-to-DM conversion (in dB) is related to the phase and/or amplitude mismatches.

The theoretical considerations are first applied on the connection cables, which cause a phase mismatch but no significant amplitude mismatch. It is calculated that for limiting the CM-to-DM conversion to -50 dB (i.e. only around 0.3 % of the generated CM noise is converted into DM noise due to the cable) a phase error of smaller than 0.18° must be achieved. At the frequency of 30 MHz (maximum frequency of the Conducted Emissions (CE) compliance test range) the 0.18° correspond to only 3.3 mm cable length mismatch. The very strict tolerance in the millimeter range highlights the importance of an absolutely symmetric test setup, as well as the sensitivity of the EMI measurements with respect to the connection cables.

Subsequently, the impact of imbalances in the LISN, which is placed between the EUT and the separator, is quantified. It is shown, by means of transfer function measurements, that the LISN causes both, phase and amplitude mismatch to the EMI noise. The worst-case CM-to-DM conversion for a given amplitude and phase mismatch is theoretically derived and experimentally measured and a reasonably good matching between the two values is observed. The CM-to-DM conversion of the LISN is significant with up to -21 dB (almost 10 % of the CM EMI noise is converted into DM noise). In order to address this problem, it is suggested to place an external high-pass filter between the LISN and the separator to measure the EMI noise. Experimental results show that this reduces the CM-to-DM conversion by at least 10 dB over a wide frequency range.

Finally, the influence of the EMI filter is analyzed. Layout mismatches and component parasitic elements can result in inherent conversion of CM noise at the filter input into DM components at the filter output terminals. This means, that even with an ideal measurement setup and a perfect noise separator, the theoretical CM and DM noise sources cannot be identified correctly. A CM noise source for example would partially appear as DM component at the separator due to the parasitic CM-to-DM conversion in the CM filter, and therefore could

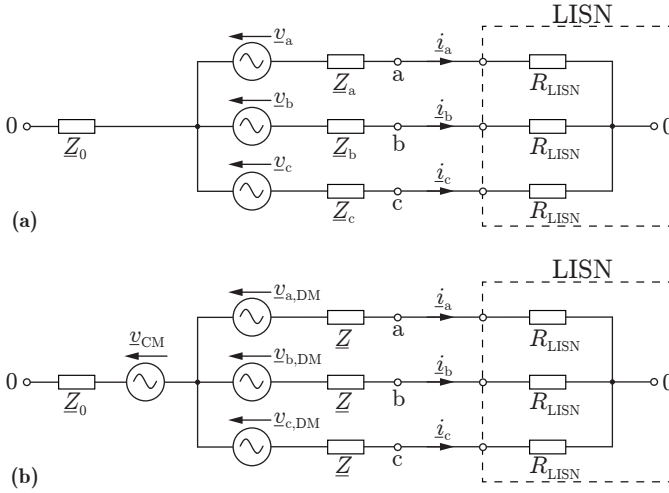


Fig. 18. (a) HF equivalent circuit of the three-phase converter with inner noise source impedances connected to the LISN and (b) decomposition into CM and DM parts.

be wrongly attributed to an insufficiently performing DM filter stage. Therefore, the importance of matched components and a symmetric layout of the EMI filters becomes evident. With a high performance noise separator such filter asymmetries and/or parasitic coupling effects that result in a CM-to-DM conversion (and vice versa) can be easily identified. For this, the filter is excited with a CM noise source and the outputs are measured with the noise separator that extracts any unwanted DM components, attributed to CM-to-DM conversion in the filter. With help of such measurements, converter simulation models can be successively improved and the predicted results become more reliable, which greatly facilitates the EMI pre-compliance testing.

As a final remark, it should be highlighted that small mismatches already have a severe impact on the CM-to-DM conversion at the upper frequency limit of 30 MHz (according to the CISPR standards). In aerospace applications for example, different norms such as the DO-160 [18] apply, which define an upper frequency limit of 152 MHz for the CE. It is clear that at such frequencies the fulfillment of the symmetry requirements is even more important as, e.g., a cable length mismatch of 4.8 cm would already result in a CM-to-DM conversion of around -16 dB (compared to -30 dB at 30 MHz, i.e., around a factor of 4 higher).

APPENDIX A

THREE-PHASE CM/DM DECOMPOSITION

Fig. 18 (a) shows a general asymmetric three-phase arrangement (v_i indicating the HF noise source of phase i , Z_i inner noise source impedance or filter circuit impedance and Z_0 capacitive coupling to ground) with the following properties:

$$v_{a,LISN} = i_a R_{LISN} = v_a - i_a Z_a - (i_a + i_b + i_c) Z_0 \quad (14)$$

$$v_{b,LISN} = i_b R_{LISN} = v_b - i_b Z_b - (i_a + i_b + i_c) Z_0 \quad (15)$$

$$v_{c,LISN} = i_c R_{LISN} = v_c - i_c Z_c - (i_a + i_b + i_c) Z_0 \quad (16)$$

Three individual noise voltages $v_{i,LISN}$, effect of a filtering measure or of specific properties of the noise sources

v_i , cannot be assessed immediately concerning the resulting $v_{i,LISN}$ (14) - (16), especially considering the typically inductive behavior of Z_i (increasing impedance with increasing frequency) and the capacitive behavior of Z_0 (decreasing impedance with increasing frequency).

Following the symmetry of the supplying three-phase mains, three-phase power electronics converter systems are built considering phase symmetry, which also ensures equal loading of the phase bridge legs. In consequence, also the filter circuits show phase symmetry (neglecting e.g. the influence of different instantaneous phase current levels on the inductance value of the phase filter inductors) and we have

$$Z_a = Z_b = Z_c = Z. \quad (17)$$

Based on (17) the leakage current to ground,

$$i_{CM} = i_a + i_b + i_c \quad (18)$$

is equally distributed to the phases and driven by a voltage component, which is equally contained in the phase noise voltages v_i and called CM voltage

$$v_{CM} = \frac{1}{3} (v_a + v_b + v_c). \quad (19)$$

Accordingly, the remaining voltages

$$v_{DM,a} = v_a - v_{CM} \quad (20)$$

$$v_{DM,b} = v_b - v_{CM} \quad (21)$$

$$v_{DM,c} = v_c - v_{CM} \quad (22)$$

with

$$v_{DM,a} + v_{DM,b} + v_{DM,c} = 0 \quad (23)$$

are driving noise currents $i_{DM,i}$, which are remaining inside the three-phase circuit arrangement, called DM noise currents. Finally, this results in a splitting of the measured noise voltage

$$v_{CM,LISN} = v_{cm} - i_{CM} \left(Z_0 + \frac{1}{3} Z \right) \quad (24)$$

$$v_{DM,LISN,i} = v_{DM,i} - i_{DM,i} \cdot Z \quad (25)$$

which is of clear advantage,

- as the composition of the noise source voltage can be directly influenced through the modulation of three-phase converter circuits,
- dedicated filter arrangements can be provided to combat a CM or DM noise problem, which is facilitated by the fact that
- the above mentioned inductive and capacitive characteristics of Z_i and Z_0 are now taking mainly influence only on one of the two noise components.

APPENDIX B

DM-TO-CM CONVERSION

As mentioned in **Section III** in a asymmetric three-phase transmission system besides the CM-to-DM conversion also the reciprocal DM-to-CM conversion takes place. Assuming a perfectly balanced three-phase DM input voltage system at the input of the asymmetric transmission system, similarly to the case of a pure CM input voltage, a certain amplitude

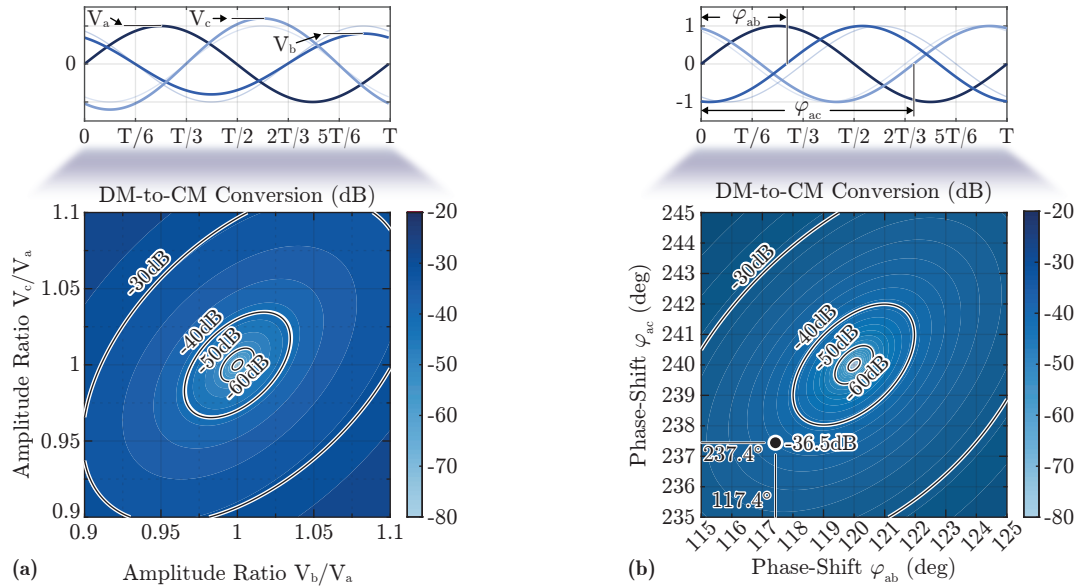


Fig. 19. Amplitude and phase mismatches at the output of an unsymmetric three-phase transmission system and related characterization of the transmission system with a DM-to-CM conversion under the assumption of a perfectly balanced three-phase DM input voltage system. For all cases, input channel a is treated as reference. **(a)** Considering only an amplitude mismatch V_b/V_a and V_c/V_a and **(b)** considering only a phase mismatch φ_{ab} and φ_{ac} .

and phase mismatch at the transmission system output results. With channel a as reference channel, there are amplitude ratios V_b/V_a and V_c/V_a as well as phase-shifts φ_{ab} and φ_{ac} . **Fig. 19** shows the DM-to-CM conversion normalized with respect to the DMTF, resulting from imperfect amplitude ratios ($V_b/V_a \neq 1$ and $V_c/V_a \neq 1$) and phase-shifts deviating from the nominal values of $\varphi_{ab} = 120^\circ$ and $\varphi_{ac} = 240^\circ$, respectively. Notable is that for the DM-to-CM conversion there exists no mutual cancellation of the amplitude and/or phase error (cf. **Fig. 9**). Therefore, indeed, for certain amplitude and/or phase error combinations, there is a more pronounced DM-to-CM conversion. However, as stated in **Section III**, for a given maximum amplitude or phase error, the worst-case DM-to-CM conversion in a three-phase system is typically less pronounced compared to the CM-to-DM conversion. This is exemplary indicated in **Fig. 19 (b)** for the point corresponding to a relative phase error of -2.6° for both, φ_{ab} and φ_{ac} . The DM-to-CM conversion results in -36.5 dB whereas for the same phase error a CM-to-DM conversion of -30.4 dB results (cf. **Fig. 9 (e)-(f)**).

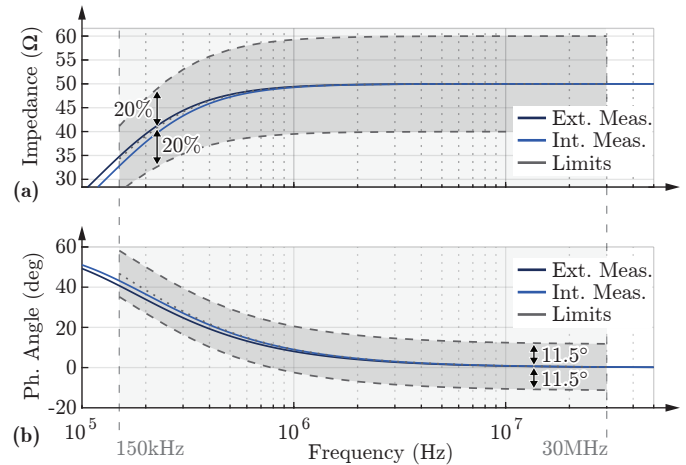


Fig. 20. LISN input impedance at the EUT port for both, internal and external HF measurement paths. **(a)** Magnitude and **(b)** phase angle, including the tolerance band around the nominal value according to CISPR 16-1-2.

APPENDIX C

LISN EUT PORT INPUT IMPEDANCE

Fig. 20 shows the LISN input impedance **(a)** magnitude and **(b)** phase angle seen at the EUT port (Z_{EUT}) for the internal and the external HF measurement paths (cf. **Section V-A** and **Section V-B**). Further depicted is the nominal value of Z_{EUT} (dotted lines) and the corresponding tolerance bands (dashed lines) according to the CISPR 16-1-2 regulations ($\pm 20\%$ for the magnitude and $\pm 11.5^\circ$ for the phase angle) [2]. This demonstrates, that even with an external HPF the setup complies with the standards.

REFERENCES

- [1] International Electrotechnical Commission (IEC), "Cispr 11: Limits and methods of measurement of electromagnetic disturbance characteristics of industrial, scientific and medical (ism) radiofrequency equipment!" Tech. Rep., 1990.
- [2] International Electrotechnical Commission (IEC), "Cispr 16: Specification for radio disturbance and immunity measuring apparatus and methods part 1-2: Radio disturbance and immunity measuring apparatus coupling devices for conducted disturbance measurements," Tech. Rep., 2015.
- [3] M. Heldwein, J. Biela, H. Ertl, T. Nussbaumer, and J. W. Kolar, "Novel three-phase cm/dm conducted emission separator," *IEEE Transactions on Industrial Electronics*, vol. 56, no. 9, pp. 3693–3703, Sep. 2009.
- [4] P. S. Niklaus, D. Bortis, and J. W. Kolar, "Design and experimental analysis of a three-phase active cm/dm conducted emi noise separator,"

accepted for the CPSS Transactions on Power Electronics and Applications, 2020.

- [5] J. Dobusch, P. Konarski, D. Kuebrich, and T. Duerbaum, "Implementation of voltage based three-phase cm/dm noise separation on the drive side," in *Proc. of the 20th European Conference on Power Electronics and Applications (EPE ECCE Europe)*, Sep. 2018, pp. P.1–P.9.
- [6] S. Wang, F. Luo, and F. C. Lee, "Characterization and design of three-phase emi noise separators for three-phase power electronics systems," *IEEE Transactions on Power Electronics*, vol. 26, no. 9, pp. 2426–2438, Sep. 2011.
- [7] A. de Beer, "Reducing common mode emi generation in a boost converter using the imbalance difference model," in *Proc. of the IEEE International Conference on Environment and Electrical Engineering (EEEIC)*, 2017, pp. P.1–P.6.
- [8] S. Wang, "Modeling and design of emi noise separators for multiphase power electronics systems," *IEEE Transactions on Power Electronics*, vol. 26, no. 11, pp. 3163–3173, 2011.
- [9] Y. Zhang, Y. Shi, and H. Li, "Emi noise separation method for three-phase wbg inverters with low sensitivity to parasitic parameters," *IEEE Transactions on Power Electronics*, vol. 33, no. 6, pp. 4589–4593, 2018.
- [10] J. Dobusch, D. Kuebrich, and T. Duerbaum, "Implementation of current based three-phase cm / dm noise separation on the drive side," in *Proc. of the International Symposium on Electromagnetic Compatibility (EMC EUROPE)*. IEEE, 2018, pp. 220–225.
- [11] P.-S. Chen and Y.-S. Lai, "Effective emi filter design method for three-phase inverter based upon software noise separation," *IEEE Transactions on Power Electronics*, vol. 25, no. 11, pp. 2797–2806, 2010.
- [12] International Electrotechnical Commission (IEC), "Cispr 16: Specification for radio disturbance and immunity measuring apparatus and methods part 1-1: Radio disturbance and immunity measuring apparatus," Tech. Rep., 2015.
- [13] Omicron Lab, "Bode100 – user manual," 2019. [Online]. Available: https://www.omicron-lab.com/fileadmin/assets/Bode_100/Manuals/Bode-100-User-Manual-ENU10060505.pdf
- [14] Pasternack, "Flexible rg58 coax cable single shielded with black pcv (nc) jacket," pp. 1–3, 2017. [Online]. Available: <https://www.pasternack.com/images/ProductPDF/RG58C-U.pdf>
- [15] Rohde & Schwarz GmbH & Co. KG, "Env216 - two line v-network," 2020. [Online]. Available: https://scdn.rohde-schwarz.com/ur/pws/dl_downloads/dl_common_library/dl_manuals/gb_1/e/env216_1/ENV216_UserManual_en_04.pdf
- [16] M. Schutten, S. Prabhakaran, D. Karipides, J. Nasadoski, and R. Thomas, "High frequency emi filter parasitic characterization," *Proc. of the IEEE Vehicle Power and Propulsion Conference (VPPC)*, no. V, pp. 1–8, 2011.
- [17] S. Wang, F. C. Lee, W. G. Odendaal, and J. D. van Wyk, "Improvement of emi filter performance with parasitic coupling cancellation," in *Proc. of the IEEE Power Electronics Specialists Conference (PESC)*. IEEE, 2005, pp. 1780–1786.
- [18] Radio Technical Commission for Aeronautics (RTCA), "Do-160: Environmental conditions and test procedures for airborne equipment," Tech. Rep., 1990.
- [19] C. R. Paul and K. B. Hardin, "Diagnosis and reduction of conducted noise emissions," *IEEE Transactions on Electromagnetic Compatibility*, vol. 30, no. 4, pp. 553–560, Nov. 1988.
- [20] Rohde & Schwarz GmbH & Co. KG, "EspI - emi test receiver specifications," 2009. [Online]. Available: https://scdn.rohde-schwarz.com/ur/pws/dl_downloads/dl_common_library/dl_brochures_and_datasheets/pdf_1/ESPI_specs_en.pdf



as a Ph.D. student focusing on advanced measurement technologies and methods in the field of power electronics.

Pascal S. Niklaus (STM'17) received his B.Sc. and M.Sc. degree (with distinction) in electrical engineering from the Swiss Federal Institute of Technology (ETH) Zurich, Switzerland, in 2016 and 2018, respectively. During his studies he did two internships where he developed hardware, firmware and software for custom and off-the-shelf test and measurement equipment as well as working on the firmware development for a new microprocessor architecture. In April 2018 he joined the Power Electronic Systems Laboratory (PES) at ETH Zurich



wide-bandgap power devices and low EMI emission profile converters.

Michael M. Antivachis (SM'10) Michael Antivachis received the B.Sc. degree in electrical engineering from National Technical University of Athens (NTUA) in 2014 and the M.Sc. degree in energy science and technology from ETH Zurich in 2016. Since June 2016 he is with the Power Electronic Systems Laboratory of ETH Zurich as a Ph.D. candidate.

His research interests include high-speed motor drive systems for commercial applications, efficient inverters topologies in a small form factor employing



Systems at PES, which concentrates on ultrahigh speed motors, magnetic bearings and bearingless drives, new linear-rotary actuator and machine concepts with integrated power electronics. Targeted applications include e.g. highly dynamic and precise positioning systems, medical and pharmaceutical systems, and future mobility concepts. Dr. Bortis has published 90+ scientific papers in international journals and conference proceedings. He has filed 30+ patents and has received 7 IEEE Conference Prize Paper Awards.

Dominik Bortis (M'08) received the M.Sc. and Ph.D. degree in electrical engineering from the Swiss Federal Institute of Technology (ETH) Zurich, Switzerland, in 2005 and 2008, respectively. In May 2005, he joined the Power Electronic Systems Laboratory (PES), ETH Zurich, as a Ph.D. student. From 2008 to 2011, he has been a Postdoctoral Fellow and from 2011 to 2016 a Research Associate with PES, co-supervising Ph.D. students and leading industry research projects. Since January 2016 he is heading the research group Advanced Mechatronic



Johann W. Kolar (F'10) received his M.Sc. and Ph.D. degree (summa cum laude / promotio sub auspiciis praesidentis rei publicae) from the University of Technology Vienna, Austria, in 1997 and 1999, respectively. Since 1984, he has been working as an independent researcher and international consultant in close collaboration with the University of Technology Vienna, in the fields of power electronics, industrial electronics and high performance drive systems. He has proposed numerous novel PWM converter topologies, and modulation and control

concepts and has supervised 70+ Ph.D. students. He has published 880+ scientific papers in international journals and conference proceedings, 4 book chapters, and has filed 190+ patents. The focus of his current research is on ultra-compact and ultra-efficient SiC and GaN converter systems, solid-state transformers, advanced variable speed three-phase motor drives, integrated modular motor drives, ultra-high speed motors, bearingless motors/actuators, and design automation in power electronics/mechatronics. Dr. Kolar has received 33 IEEE Transactions and Conference Prize Paper Awards, the 2014 IEEE Middlebrook Award, the 2016 IEEE William E. Newell Power Electronics Award, the 2016 IEEE PEMC Council Award and two ETH Zurich Golden Owl Awards for excellence in teaching. He initiated and/or is the founder of four ETH Spin-off companies. He is a member of the steering committees of several leading international conferences in the field and has served from 2001 through 2013 as an Associate Editor of the IEEE Transactions on Power Electronics. Since 2002 he also is an Associate Editor of the Journal of Power Electronics of the Korean Institute of Power Electronics and a member of the Editorial Advisory Board of the IEEJ Transactions on Electrical and Electronic Engineering.